Intact piRNA pathway prevents L1 mobilization in male meiosis

Simon J. Newkirk[a,b], Suman Lee[a], Fiorella C. Grandi[b,1], Valeriya Gaysinskaya[c], James M. Rosser[b,2], Nicole Vanden Berg[a], Cathryn A. Hogarth[b], Maria C. N. Marchetto[d], Alysson R. Muotri[d,3], Michael D. Griswold[b], Ping Ye[e,f], Alex Bortvin[c], Fred H. Gage[d,4], Jef D. Boeke[g], and Wenfeng An[a,4]

[a]Department of Pharmaceutical Sciences, South Dakota State University, Brookings, SD 57007; [b]School of Molecular Biosciences, Washington State University, Pullman, WA 99164; [c]Department of Embryology, Carnegie Institution of Washington, Baltimore, MD 21218; [d]Laboratory of Genetics, Salk Institute for Biological Studies, La Jolla, CA 92037; [e]Department of Molecular and Experimental Medicine, Avera Cancer Institute, Sioux Falls, SD 57105; [f]Department of Pharmacy Practice, South Dakota State University, Brookings, SD 57007; and [g]Institute for Systems Genetics, New York University Langone Medical Center, New York, NY 10016

Contributed by Fred H. Gage, May 24, 2017 (sent for review January 26, 2017; reviewed by Prescott Deininger and P. Jeremy Wang)

The PIWI-interacting RNA (piRNA) pathway is essential for retrotransposon silencing. In piRNA-deficient mice, L1-overexpressing male germ cells exhibit excessive DNA damage and meiotic defects. It remains unknown whether L1 expression simply highlights piRNA deficiency or actually drives the germ-cell demise. Specifically, the sheer abundance of genomic L1 copies prevents reliable quantification of new insertions. Here, we developed a codon-optimized L1 transgene that is controlled by an endogenous mouse L1 promoter. Importantly, DNA methylation dynamics of a single-copy transgene were indistinguishable from those of endogenous L1s. Analysis of *Mov10l1*$^{-/-}$ testes established that de novo methylation of the L1 transgene required the intact piRNA pathway. Consistent with loss of DNA methylation and programmed reduction of H3K9me2 at meiotic onset, the transgene showed 1,400-fold increase in RNA expression and consequently 70-fold increase in retrotransposition in postnatal day 14 *Mov10l1*$^{-/-}$ germ cells compared with the wild-type. Analysis of adult *Mov10l1*$^{-/-}$ germ-cell fractions indicated a stage-specific increase of retrotransposition in the early meiotic prophase. However, extrapolation of the transgene data to endogenous L1s suggests that it is unlikely insertional mutagenesis alone accounts for the *Mov10l1*$^{-/-}$ phenotype. Indeed, pharmacological inhibition of reverse transcription did not rescue the meiotic defect. Cumulatively, these results establish the occurrence of productive L1 mobilization in the absence of an intact piRNA pathway but leave open the possibility of processes preceding L1 integration in triggering meiotic checkpoints and germ-cell death. Additionally, our data suggest that many heritable L1 insertions originate from individuals with partially compromised piRNA defense.

LINE-1 reporter transgene | meiotic arrest | PIWI-interacting RNA | retrotransposition | spermatogenesis

The bulk of mammalian genomes are made up of transposable elements, the majority of which are retrotransposons (1). Retrotransposons are classified into long-interspersed elements (LINEs), short-interspersed elements (SINEs), and LTR retrotransposons, which collectively account for 43% and 37% of the human and mouse genomes, respectively (2). Retrotransposons amplify in the genome through an RNA intermediate, a process termed retrotransposition. LINEs are autonomous elements. An intact, full-length LINE-1 (L1) encodes two ORFs (i.e., ORF1 and ORF2); both are required for L1 mobilization (3). SINEs are nonautonomous elements and rely on L1's proteins for propagation in the genome (4). LTR retrotransposons are autonomous but appear to be inactivated in the human genome (5). Retrotransposition endangers the integrity of both somatic and germline genomes through insertional mutagenesis. In somatic tissues, both elevated L1 expression and retrotransposition have been strongly associated with many types of human cancers (6, 7). In a few cases, specific retrotransposition events (i.e., insertions) have been determined to drive tumorigenesis (8, 9). In the germline, retrotransposon insertions are responsible for sporadic cases of human genetic diseases, including hemophilia A (10) and neurofibromatosis 1 (11).

Maintaining germline integrity is crucial for passing accurate genetic information to the next generation. Indeed, recent studies have uncovered an intricate network of defense mechanisms that mammalian germ cells use to control retrotransposon activities (12, 13). Chief among them is the transcriptional and posttranscriptional silencing of retrotransposons by the PIWI-interacting RNA (piRNA) and DNA methylation pathway. piRNAs are 24- to 31-nt-long small RNAs that are predominantly expressed during two distinct phases of male germ-cell development. The first phase is in prospermatogonia of fetal testes. These "fetal piRNAs" are associated with mouse PIWI proteins MILI and MIWI2, and are enriched for retrotransposon sequences (14, 15). Fetal piRNAs are expressed during the period of DNA methylation reprogramming in the mouse germline and play a critical role in transcriptional silencing of retrotransposons. Recent data support a model in which

Significance

Retrotransposons make up the bulk of the human genome and, if unleashed, threaten the genomic integrity through DNA damage and insertional mutagenesis. In germ cells, an intact PIWI-interacting RNA pathway is essential for suppressing the expression of L1 retrotransposons. Deficiencies in the PIWI-interacting RNA pathway have dire consequences because mutant males are invariably sterile. To address the role of retrotransposon activation in these mutants, we developed an L1 reporter transgenic mouse. This mouse model allowed us to detect significant and stage-specific increases of new insertions in mutant germ cells, to draw attention to the importance of other L1-related activities for germ-cell health, and to predict the timing and origin of heritable L1 insertions in the human population.

Author contributions: S.J.N. and W.A. designed research; S.J.N., S.L., F.C.G., J.M.R., N.V.B., M.C.N.M., A.R.M., and W.A. performed research; V.G. and A.B. contributed new reagents/analytic tools; S.J.N., S.L., F.C.G., J.M.R., C.A.H., M.D.G., P.Y., F.H.G., J.D.B., and W.A. analyzed data; F.H.G., J.D.B., and W.A. directed model development; and S.J.N. and W.A. wrote the paper.

Reviewers: P.D., Tulane Cancer Center; and P.J.W., University of Pennsylvania.

The authors declare no conflict of interest.

Freely available online through the PNAS open access option.

See Commentary on page 7194.

[1]Present address: Cancer Biology Program, Stanford University, Stanford, CA 94305.

[2]Present address: ReachBio LLC, Seattle, WA 98107.

[3]Present addresses: Department of Pediatrics, University of California, San Diego, La Jolla, CA 92093; and Department of Cellular & Molecular Medicine, University of California, San Diego, La Jolla, CA 92093.

[4]To whom correspondence may be addressed. Email: gage@salk.edu or wenfeng.an@sdstate.edu.

This article contains supporting information online at www.pnas.org/lookup/suppl/doi:10.1073/pnas.1701069114/-/DCSupplemental.

retrotransposon-derived piRNAs serve as a guide to selectively target young L1 families for de novo DNA methylation (16) or H3K9me3 modification (17). Functional deletion of many cofactors in the piRNA-DNA methylation pathway leads to abnormal L1 expression accompanied by the loss of DNA methylation at L1 promoters (12, 13). The second phase peaks in pachytene spermatocytes. These "pachytene piRNAs" are associated with mouse PIWI proteins MILI and MIWI, relatively depleted of retrotransposon sequences, and expressed from genomic clusters. The pachytene piRNA pathway posttranscriptionally regulates coding/noncoding RNAs and retrotransposons (18–20). Accordingly, L1 expression is elevated in *Miwi*-deficient testes (19, 21).

A functional deficiency in the piRNA-DNA methylation pathway exerts devastating consequences on mouse germ-cell development. Afflicted males are invariably sterile because of spermatogenic failures. In addition, the majority of the mutants suffer meiotic arrest, accompanied by excessive DNA damage and numerous meiotic defects (12, 13). A fundamental unanswered question in germ-cell biology is whether the elevated L1 expression simply highlights piRNA deficiency or actually drives the germ-cell demise. One of the hypotheses is that loss of retrotransposon control at the transcriptional and posttranscriptional level would lead to massive insertional mutagenesis in developing germ cells, which would be subsequently eliminated through apoptosis (12, 13). In principle, this hypothesis can be tested by measuring the level of new insertions in the piRNA pathway-deletion mutants. However, the sheer abundance of preexisting L1 copies in the mouse genome presents a formidable technical challenge to quantifying the frequency and magnitude of de novo insertions. Indeed, this technical barrier has prevented the characterization of the extent and timing of retrotransposition during germ-cell development (22). For example, even the most rudimentary information is unavailable as to what extent retrotransposition occurs in piRNA pathway mutants and whether an increase of insertions, if any, is concurrent with the meiotic phenotype.

To overcome this hurdle, we resorted to reporter transgenes, which offer an alternative approach to direct quantification of endogenous retrotransposons. L1 transgenes carrying a retrotransposition indicator cassette have been previously used to track de novo L1 insertions in mouse models (23–29). However, the majority of these mouse models used human L1-based transgenes or constitutively active non-L1 promoters. The current model suggests a sequence-specific interaction between a piRNA and its target for transcriptional (30, 31) and posttranscriptional silencing (19, 32, 33). Thus, we reasoned that an L1 transgene with an endogenous mouse L1 promoter is the best way to model L1 regulation by the piRNA-DNA methylation pathway. Here we describe the validation of such a transgene and the characterization of L1 retrotransposition in *Mov10l1*$^{-/-}$ mice.

Results

Developing an L1 Transgene Regulated by the Endogenous Mouse L1 Promoter. To establish a transgenic mouse model through which L1 regulation, expression, and mobilization could be queried, we constructed a mouse L1 transgene, 5′UTR-ORFeus (Fig. 1*A*; detailed in Fig. S1*A*). The significant attributes of the transgene are: (*i*) an endogenous mouse L1 promoter, (*ii*) codon-optimized mouse L1 ORF1 and ORF2 sequences, and (*iii*) an EGFP-based retrotransposition indicator cassette. The endogenous L1 5′UTR promoter is derived from L1spa (34), an active Tf family element that inserted within intron 6 of the glycine receptor β-subunit, causing muscular spasticity in the *spastic* mouse. The codon-optimized ORF1 and ORF2 sequences are from ORFeus-Mm, which supports efficient transcription elongation (35) and consequently higher retrotransposition both in vitro (36) and in vivo (25). The intron-disrupted EGFP cassette has been used to report retrotransposition in vivo (26, 28). Through pronuclear microinjection, we produced three independent transgenic mouse lines. We determined the transgene copy number using qPCR and found that the copy number varied at 1, 14, and 22 tandem repeats (hereafter referred to as SN1, SN14, and SN22, respectively) (Fig. S1*C*). The copy number did not change from generation to generation, suggesting that each carried the transgenic sequence at a single locus and was relatively stable. Using ligation-mediated PCR, we mapped the single-copy transgene in line SN1 to the first intron of the mouse tenascin R (*Tnr*) gene locus on chromosome 1 (Fig. S1*D*). TNR expression is restricted to the CNS (37). Mice homozygous for the SN1 transgene were viable and fertile. However, whether the integration of the transgene affects *Tnr* function in the brain is unknown.

Single-Copy L1 Transgene Recapitulates Endogenous DNA Methylation Dynamics. The germline genome is epigenetically reprogrammed during fetal development. In particular, L1 5′UTR sequences are rapidly demethylated in wild-type mouse primordial germ cells between E10.5 and E13.5 (38) and later remethylated in prospermatogonia by E17.5 (39). To determine whether the promoter of the L1 transgene recapitulates the methylation dynamics of

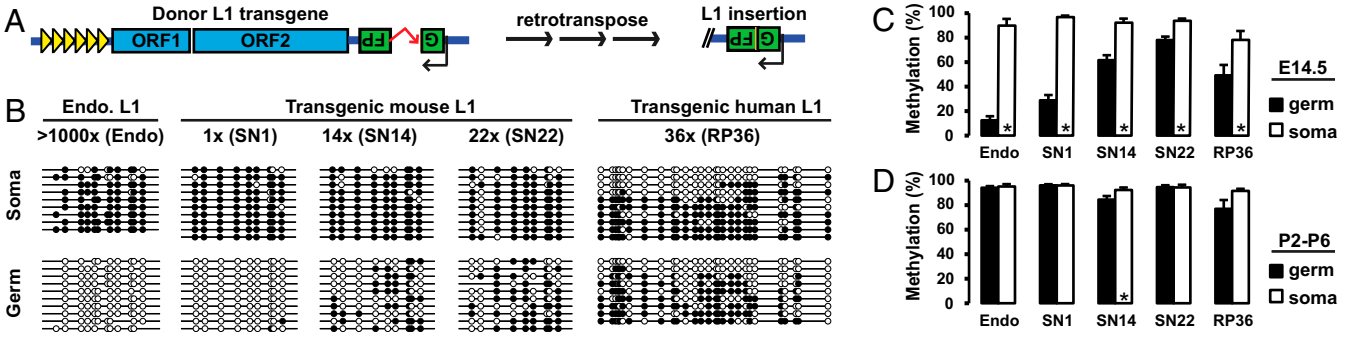

Fig. 1. The single-copy mouse L1 transgene recapitulates endogenous methylation dynamics. (*A*) Sequence features of the 5′UTR-ORFeus transgene. The transgene is transcriptionally regulated by an endogenous mouse L1 5′UTR promoter, which comprises multiple copies of tandem monomers (illustrated as triangles). The EGFP-based retrotransposition indicator cassette is coded by the antisense strand of the transgene. It contains a sense-oriented intron, which would be spliced during retrotransposition. The resulting EGFP insertion would lack the intron (shown as 5′ truncated). (*B*) DNA methylation dot plots of endogenous and transgenic L1 promoter sequences in testicular somatic and germ cells from E14.5 embryos. Up to 10 bisulfite sequencing reads are displayed for each genotype. The entire dataset is included in Fig. S2 and summarized in *C*. Open and filled circles represent unmethylated and methylated CpGs, respectively. (*C*) Endogenous and transgenic L1 promoter methylation in sorted somatic and germ cells from embryonic gonads. (*D*) Endogenous and transgenic L1 promoter methylation in sorted somatic and germ cells from neonatal testes. Error bars in *C* and *D* represent SEM between individual sequences. Asterisks indicate statistical difference between somatic and germ cells (Mann–Whitney *U* test, $P < 0.05$). endo, endogenous; soma, somatic.

endogenous L1s, we analyzed transgene promoter methylation by bisulfite sequencing and compared the results to endogenous L1s in E14.5 embryos (normally hypomethylated) and in neonatal animals (normally hypermethylated). To analyze specifically the somatic and germ cells within the testis, we crossed our transgenes with an OCT4-EGFP transgene (40) and collected GFP^+ (germ cells) and GFP^- (testicular somatic cells) fractions through FACS. To target the 5′UTR of the transgene, a 650-bp region was amplified with a forward primer in the 5′UTR and a reverse primer anchored in the codon-optimized ORF1 sequence (Fig. S1*A*). In contrast, the 5′UTR of endogenous L1s was amplified with a pair of forward and reverse primers in the 5′UTR (Fig. S1*B*). Unexpectedly, the high-copy donor transgenes (SN14 and SN22) appeared to resist global demethylation and remained highly methylated in E14.5 male germ cells (61.6% and 78.1%, respectively). In contrast, the single-copy transgene (SN1; 28.8%) showed considerable hypomethylation, and was most similar to the endogenous methylation status (12.5%) in E14.5 germ cells (Fig. 1 *B* and *C*). The control testicular somatic cells showed high levels of methylation for both endogenous and transgenic L1 promoters in E14.5 germ cells (Fig. 1 *B* and *C*). Interestingly, all transgenes displayed an expected hypermethylation profile in testicular somatic and germ cells after birth (Fig. 1*D* and Fig. S2).

As a comparison, we analyzed the methylation status of the promoter of a human L1RP-based transgene (26). This transgene was integrated into the mouse genome as a tandem array of 36 copies (RP36 hereafter) (Fig. S1*C*). Its methylation status was quite similar to high-copy 5′UTR-ORFeus transgenes, showing a relatively high level of methylation in E14.5 germ cells (49.2%) (Fig. 1 *B* and *C*). However, unlike the transgenic mouse L1 promoter, the human L1 promoter had fully unmethylated reads both in E14.5 testicular somatic cells and in postnatal germ cells (Fig. 1*B* and Fig. S2). It remains undetermined why tandem-arrayed L1 transgenes were less efficiently demethylated in prospermatogonia. To avoid any unknown confounding factors related to tandem-arrayed sequences, the single-copy SN1 transgene was used for the remainder of the study.

Retrotransposition Is Increased in *Mov10l1*-Deficient Adult Mice. To test whether our 5′UTR-ORFeus transgene was regulated by the fetal piRNA pathway, we introduced the transgene into a *Mov10l1*-deficient genetic background (41). MOV10L1 is an RNA helicase essential for primary piRNA biogenesis (42). Global deletion of *Mov10l1* leads to the loss of fetal piRNAs and male-specific meiotic defects, which are accompanied by L1 hypomethylation and up-regulation at both RNA and protein levels in postnatal $Mov10l1^{-/-}$ testes (41, 43). In agreement with these previous reports, the endogenous L1s were hypomethylated in adult $Mov10l1^{-/-}$ mouse testes, with methylation reduced from 93.8 to 28.7% ($P < 0.001$) (Fig. 2 *A* and *B*). In comparison, the 5′ UTR of the SN1 transgene showed a reduction in methylation from 95.9 to 49.0% ($P < 0.001$). When bisulfite reads were examined individually, they could be grouped into two distinct populations: one population methylated at 0–20% and the other methylated at 80–100% (Fig. 2*A*). Because the piRNA pathway was not expected to affect somatic cells, we hypothesized that the hypomethylated reads originated from germ cells, whereas the hypermethylated reads came from testicular somatic cells, a hypothesis later validated by analysis of testicular cell fractions using cell sorting. Consistent with the loss of remethylation was a 7.5-fold increase of 5′UTR-ORFeus transcripts in $Mov10l1^{-/-}$ testes compared with $Mov10l1^{+/-}$ controls ($P = 0.019$) (Fig. 2*C*). Similarly, a 3.8-fold increase was detected for endogenous L1s between the two genotypes ($P = 0.002$) (Fig. 2*D*). Note, however, the qRT-PCR experiment would not discriminate between authentic

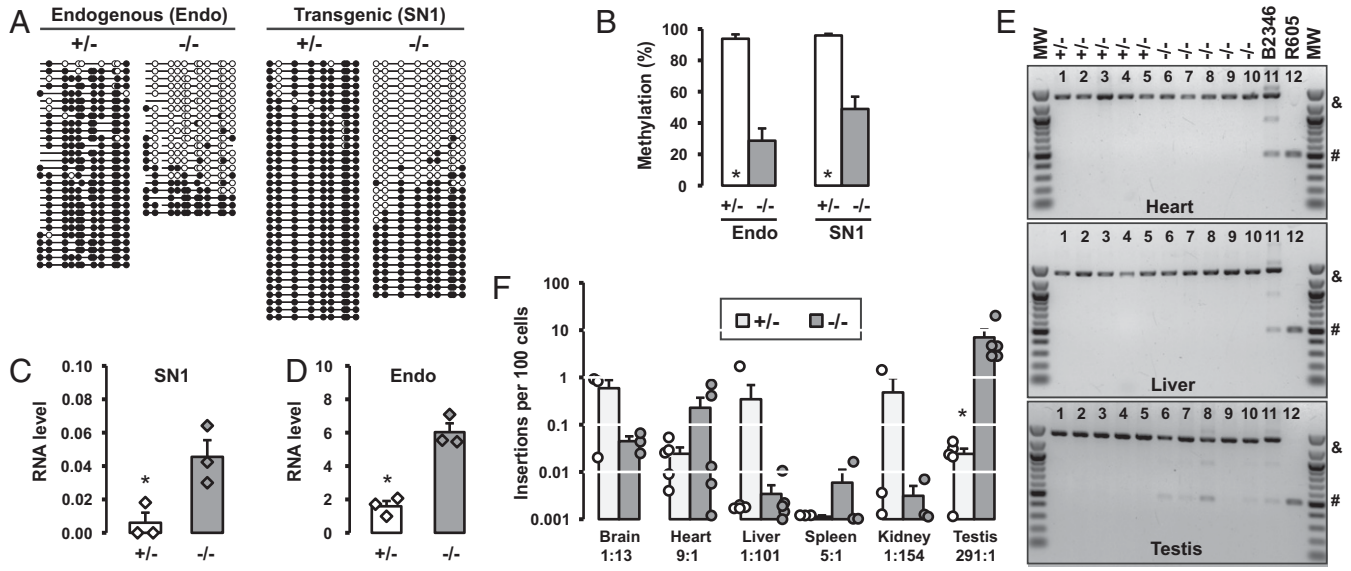

Fig. 2. Characterization of the single-copy 5′UTR-ORFeus transgene in adult mice. (*A*) DNA methylation dot plots of endogenous and transgenic L1 promoter sequences in $Mov10l1^{+/-}$ and $Mov10l1^{-/-}$ adult testes. (*B*) Histogram representation of methylation data from *A*. Endo, endogenous L1 promoter; SN1, the promoter of the single-copy 5′UTR-ORFeus transgene. Error bars represent SEM between individual sequences. Asterisks indicate statistical difference between two genotypes (Mann–Whitney *U* test, $P < 0.05$). (*C*) SN1 transgene RNA in $Mov10l1^{+/-}$ and $Mov10l1^{-/-}$ adult testes. Normalized to *Gapdh* RNA abundance. Values for individual animals are indicated (diamonds). (*D*) Endogenous L1 RNA in $Mov10l1^{+/-}$ and $Mov10l1^{-/-}$ adult testes. Error bars in *C* and *D* represent SEM for biological replicates. Asterisks indicate statistical difference between two genotypes (Student's *t* test, $P < 0.05$). (*E*) Detection of retrotransposition in heart, liver, and testicular samples by intron removal PCR. Lanes 1–5, $Mov10l1^{+/-}$ mice; lanes 6–10, $Mov10l1^{-/-}$ mice; lanes 11–12, positive control animals (see main text). MW, 100 bp DNA ladder (New England Biolabs). The top 1,400-bp band ("&") corresponds to the intron-containing donor transgene. The bottom 500-bp band ("#") corresponds to intronless insertions. The gel images are color-inverted. (*F*) Insertion frequency of the transgene in a tissue panel from $Mov10l1^{+/-}$ and $Mov10l1^{-/-}$ adult mice. The insertion ratio of $Mov10l1^{-/-}$ to $Mov10l1^{+/-}$ is annotated for each tissue. ddPCR readouts for individual animals are indicated (circles). Error bars represent SEM for biological replicates. Asterisks indicate statistical difference between two genotypes (Mann–Whitney *U* test, $P < 0.05$). MW, molecular weight marker.

endogenous L1 transcripts and those cotranscribed within genes (44), and should thus be interpreted with caution (*Discussion*).

To examine the impact of a dysfunctional piRNA pathway on retrotransposition, we performed standard end-point PCR with intron-flanking primers (Fig. 2*E*). Two positive controls were included. The first was from a mouse (B2346) carrying a constitutively active CAG-ORFeus transgene, which retrotransposed at ~0.4 insertions per cell in most tissues (25). The second control was from a mouse (R605) carrying a germline insertion that had been segregated from the donor transgene (45). Both positive controls showed robust PCR signals at the expected amplicon size in the heart, liver, and testis (Fig. 2*E*). In contrast, none of the somatic tissues, regardless of the genotype, showed appreciable amplicons corresponding to L1 insertions. Remarkably, the sole exception was in *Mov10l1*$^{-/-}$ testes, which consistently produced intronless bands, albeit at varied intensities (Fig. 2*E*).

To quantitatively compare levels of SN1 retrotransposition in *Mov10l1*$^{+/-}$ and *Mov10l1*$^{-/-}$ animals, we developed a highly sensitive droplet digital PCR (ddPCR) assay using a TaqMan probe targeting the exon–exon junction of the EGFP DNA sequence (Fig. S1*A*). In this assay, each sample was partitioned into ~20,000 droplets, which were independently amplified for 40 cycles and then counted as either positive or negative based on the fluorescent intensity in each droplet (46). The reaction was duplexed with *Hprt*, an endogenous reference that is present in males as a single copy on the X chromosome. Compared with real-time PCR (47) (Fig. S3*A*), ddPCR was much more sensitive. In fact, ddPCR extended the sensitivity of detection by >1,000-fold and permitted absolute quantification of SN1 insertions in as few as one insertion in every 100,000 cells (Fig. S3*B*). The level of SN1 retrotransposition was highly variable from tissue to tissue in both genotypes (Fig. 2*F*). In *Mov10l1*$^{+/-}$ somatic tissues surveyed, the average frequency of retrotransposition was the highest in brain (0.6 insertions per 100 cells), followed by kidney (0.5 insertions per 100 cells), liver (0.3 insertions per 100 cells), and heart (0.02 insertions per 100 cells). No significant changes in retrotransposition were observed in corresponding *Mov10l1*$^{-/-}$ somatic tissues. In contrast to somatic tissues, the testis showed a 291-fold increase in retrotransposition in the *Mov10l1*$^{-/-}$ background (7.0 insertions per 100 cells) compared with that in the *Mov10l1*$^{+/-}$ background (0.02 insertions per 100 cells; $P = 0.012$) (Fig. 2*F*).

Increase in Retrotransposition Occurs During the First Wave of Spermatogenesis. Like many other piRNA pathway mutations, the spermatogenic defect in *Mov10l1*$^{-/-}$ mice is first manifested in the prophase of meiosis I, during which germ cells fail to progress from zygotene spermatocytes to pachytene spermatocytes (41, 43). To check whether there is a correlation between L1 retrotransposition and the meiotic phenotype, we queried weekly time points, starting at birth through the first wave of spermatogenesis. In *Mov10l1*$^{+/-}$ testes, the average insertion frequency varied at low levels, ranging from 0.001 to 3.3 per 100 cells (Fig. 3*A*). In *Mov10l1*$^{-/-}$ testes, the insertion frequency stayed within this range at postnatal day 0 (P0) and P7 ($P = 0.17$ and 0.44, respectively). However, from P14 and on, the minimum insertion frequency was increased to 2.0 per 100 cells in *Mov10l1*$^{-/-}$ testes. Overall, the average insertion frequency increased by 70-fold at P14 (from 0.17 to 12.0 insertions per 100 cells; $P < 0.001$), by 71-fold at P21 (from 0.14 to 10.2 insertions per 100 cells; $P < 0.001$), and by 291-fold at P28 (from 0.02 to 7.0 insertions per 100 cells; $P < 0.001$) (Fig. 3*A*). These results suggest that the loss of *Mov10l1* function instigated an upsurge in L1 retrotransposition between the P7 and P14 time points.

We reasoned that the increase in retrotransposition might be a consequence of elevated SN1 expression in *Mov10l1*$^{-/-}$ germ cells. For endogenous L1s, previous studies reported a modest increase of RNA abundance in *Mov10l1*$^{-/-}$ testes at P10 and additional increases at P12 and P14 (41, 43), but P7 testes were not examined. Using a primer pair targeting endogenous mouse L1, we compared levels of endogenous L1 RNA between the two genotypes. We observed a 16.2-fold increase at P14 in *Mov10l1*$^{-/-}$ testes ($P = 0.018$) but no change was detected at P7 ($P = 0.90$) (Fig. 3*B*). For the SN1 transgene, we used primers and a probe specific to the codon-optimized ORF2 sequence. Similar to endogenous L1s, the transgene displayed substantial increases at P14, P21, and P28 in *Mov10l1*$^{-/-}$ testes (1,403-, 443-, and 474-fold over *Mov10l1*$^{+/-}$; $P = 0.039$, 0.030, and 0.029, respectively). However, unlike endogenous L1s, which showed no change in RNA abundance at P7, the SN1 transgene had already manifested a 37-fold increase of transcripts at P7, albeit the difference was not statistically significant ($P = 0.068$) (Fig. 3*C*). Furthermore, the level of SN1 RNA was similar in P0 and P7 *Mov10l1*$^{-/-}$ testes.

To examine transgene expression at the cellular level, we adopted an in situ RNA hybridization technique termed RNAscope (48). The probe was designed to specifically target the codon-optimized ORF1 sequence (Fig. S1). At P7, both *Mov10l1*$^{+/-}$ and *Mov10l1*$^{-/-}$ testes showed negligible amount of transgenic RNA signal. However, at P14 a fraction of the *Mov10l1*$^{-/-}$ tubules displayed robust expression (Fig. 3*D*). Although the exact spermatogenic stages could not be resolved for RNAscope tissue sections, the most consistent expression was found in early spermatocytes just before the meiotic arrest (Fig. 3*D*).

Changes in endogenous and transgenic L1 RNA during the first wave of spermatogenesis were corroborated by analyses of L1 ORF1p abundance. In control *Mov10l1*$^{+/-}$ testes, Western blot analysis detected low levels of ORF1p at P14 and P21 but little signal at P0 and P7 (Fig. 3*E*), in agreement with a previous report (49). In contrast, significant increase in ORF1p was found in *Mov10l1*$^{-/-}$ testes at all time points (Fig. 3*E*). Fold-changes were modest at P0, P7, and P21 (6.5-, 6.6-, and 9.8-fold; $P = 0.020$, 0.011 and 0.001, respectively). The most profound change was observed at P14 (44-fold increase in *Mov10l1*$^{-/-}$ compared with the *Mov10l1*$^{+/-}$ background; $P = 0.013$) (Fig. 3*F*). At the cellular level, immunofluorescence analysis of testicular cross sections identified not only higher number of ORF1p^{+} cells in the *Mov10l1*$^{-/-}$ background but also with more intense staining (Fig. 3*G* and Fig. S4). Specifically, many prospermatogonia and spermatogonia (Spg) were strongly stained at P0 and P7, respectively. At P14, most tubules with leptotene/zygotene (L/Z) spermatocytes were intensely stained, and tubules with preleptotene spermatocytes were modestly stained (Fig. 3*G*).

Increased L1 expression has been attributed to lack of remethylation and subsequent loss of transcriptional silencing of endogenous L1s (41). A reduction of methylation from 84 to 72% at P10 testes and more pronounced reduction at P14 (from 85 to 54%) were previously reported (41). For the SN1 transgene, we observed a similar magnitude of reduction at P14 (from 98 to 65%; $P < 0.001$) as well as at P21 (from 91 to 53%; $P = 0.004$). More prominent reduction was seen at P28 (from 97 to 31%; $P < 0.001$) (Fig. 3*H* and Fig. S5*A*). In contrast, no reduction was seen at P0 and P7, when whole testes were analyzed. Similar methylation dynamics were detected at endogenous L1 promoters (Fig. 3*I* and Fig. S5*B*). However, L1 hypermethylation in *Mov10l1*$^{-/-}$ testes at these early time points likely reflected the lower abundance of germ cells relative to testicular somatic cells at P0 and P7 (50) rather than hypermethylation in germ cells per se (see the analysis of sorted germ cells, below).

Retrotransposition Is Increased in *Mov10l1*$^{-/-}$ Testes at the Onset of Meiosis. To further define stage-specific L1 regulation, we isolated different spermatogenic stages of germ cells from adult testes using FACS with Hoechst staining (51) (Fig. S6). The cell fractions obtained were testicular somatic cells, Spg, L/Z spermatocytes, and pachytene/diplotene (P/D) spermatocytes (the latter for *Mov10l1*$^{+/-}$ only). *Mov10l1*$^{+/-}$ and *Mov10l1*$^{-/-}$ mice exhibited similar Spg and leptotene cell profiles (Fig. 4*A*). However, no typical zygotene spermatocytes were found in the L/Z fraction from *Mov10l1*$^{-/-}$

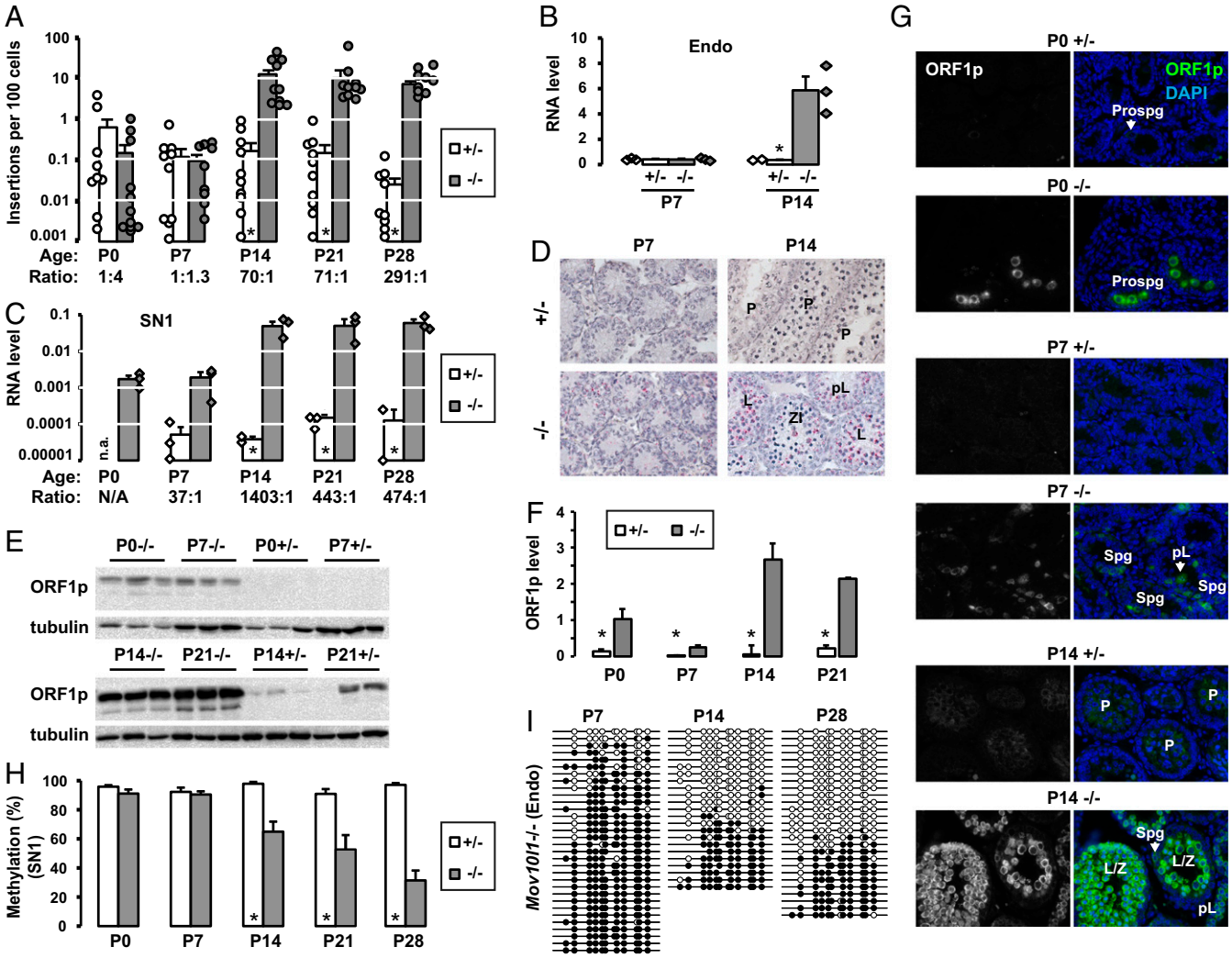

Fig. 3. Characterization of the single-copy 5′UTR-ORFeus transgene in prepuberal testes. (*A*) Insertion frequency of the transgene in prepuberal *Mov10l1*$^{+/-}$ and *Mov10l1*$^{-/-}$ testes. The age of the animals and the insertion ratio of *Mov10l1*$^{-/-}$ to *Mov10l1*$^{+/-}$ are indicated on the *x* axis. ddPCR readouts for individual animals are indicated (circles). Error bars represent SEM for biological replicates. Asterisks indicate statistical difference between two genotypes (Mann–Whitney *U* test, $P < 0.05$). (*B*) Endogenous L1 RNA in prepuberal *Mov10l1*$^{+/-}$ and *Mov10l1*$^{-/-}$ testes. Normalized to *Gapdh* RNA abundance. Values for individual animals are indicated (diamonds). (*C*) SN1 transgene RNA in prepuberal *Mov10l1*$^{+/-}$ and *Mov10l1*$^{-/-}$ testes. The RNA ratio of *Mov10l1*$^{-/-}$ to *Mov10l1*$^{+/-}$ is annotated for each age group. Error bars in *B* and *C* represent SEM for biological replicates. Asterisks indicate statistical difference between two genotypes (Student's *t* test, $P < 0.05$). N.A., not assayed. (*D*) Transgene RNA expression in prepuberal *Mov10l1*$^{+/-}$ and *Mov10l1*$^{-/-}$ testes analyzed by RNAscope. RNA targets were detected as discrete red foci. Nuclei were counterstained with Gill's hematoxylin in blue. L, leptotene; P, pachytene; pL, preleptotene; Zl, zygotene-like. (Magnification: 20×.) (*E*) Western blot analysis of ORF1p in prepuberal *Mov10l1*$^{+/-}$ and *Mov10l1*$^{-/-}$ testes. (*F*) Quantification of ORF1p in *E*. Normalized to α-tubulin. Error bars represent SEM for biological replicates. Asterisks indicate statistical difference between two genotypes (Student's *t* test, $P < 0.05$). (*G*) Immunofluorescence staining of ORF1p in prepuberal *Mov10l1*$^{+/-}$ and *Mov10l1*$^{-/-}$ testicular cross sections. P, pachytene; pL, preleptotene; Prospg, prospermatogonia. Isotype controls as well as single-channel images for DAPI are in Fig. S4. (Magnification: 20×.) (*H*) DNA methylation histograms of transgenic L1 promoter in prepuberal *Mov10l1*$^{+/-}$ and *Mov10l1*$^{-/-}$ testes. Error bars represent SEM between individual sequences. Asterisks indicate statistical difference between two genotypes (Mann–Whitney *U* test, $P < 0.05$). The corresponding methylation dot blots are in Fig. S5*A*. (*I*) Methylation dot blots of the endogenous promoter in *Mov10l1*$^{-/-}$ testes at selected time points. The complete dataset is in Fig. S5*B*. endo, endogenous.

mice. Besides leptotene spermatocytes, this fraction was enriched in defective meiotic cells with high levels of phosphorylated histone H2AX (γH2AX) but minimal SYCP3 staining. Close examination by DAPI and γH2AX labeling suggested that *Mov10l1* mutant germ cells reached leptotene to zygotene transition. Accordingly, *Mov10l1*$^{-/-}$ mice lacked P/D spermatocytes (Fig. S6*D*), consistent with previous histological analyses (41, 43).

Bisulfite sequencing analysis of sorted cells revealed that the loss of methylation had already occurred in Spg. Cells from both Spg and L/Z fractions were nearly devoid of methylation in *Mov10l1*$^{-/-}$ testes (9.8% and 7.4% methylation, respectively) (Fig. 4 *B* and *C* and Fig. S7). In contrast, the transgene promoter was almost completely methylated in corresponding fractions from *Mov10l1*$^{+/-}$ testes (96.7% and 98.1%, respectively) ($P < 0.001$ between genotypes). Identical results were obtained for endogenous L1 promoter sequences ($P < 0.001$ between genotypes) (Fig. 4 *D* and *E* and Fig. S7). Despite comparable levels of hypomethylation between Spg and spermatocytes in *Mov10l1*$^{-/-}$ mice, a consistent increase in retrotransposition occurred only in meiotic cells among different biological replicates, amounting to a 144-fold increase (from 0.02 to 3.3 insertions per 100 cells; $P = 0.031$) (Fig. 4*F*). An unexpected sevenfold increase in retrotransposition was observed in testicular somatic cell fractions (from 0.13 to 0.92 insertions per 100 cells; $P = 0.23$) (Fig. 4*F*). However, this increase in the *Mov10l1*$^{-/-}$ background could be largely attributed to the presence of one testicular somatic cell

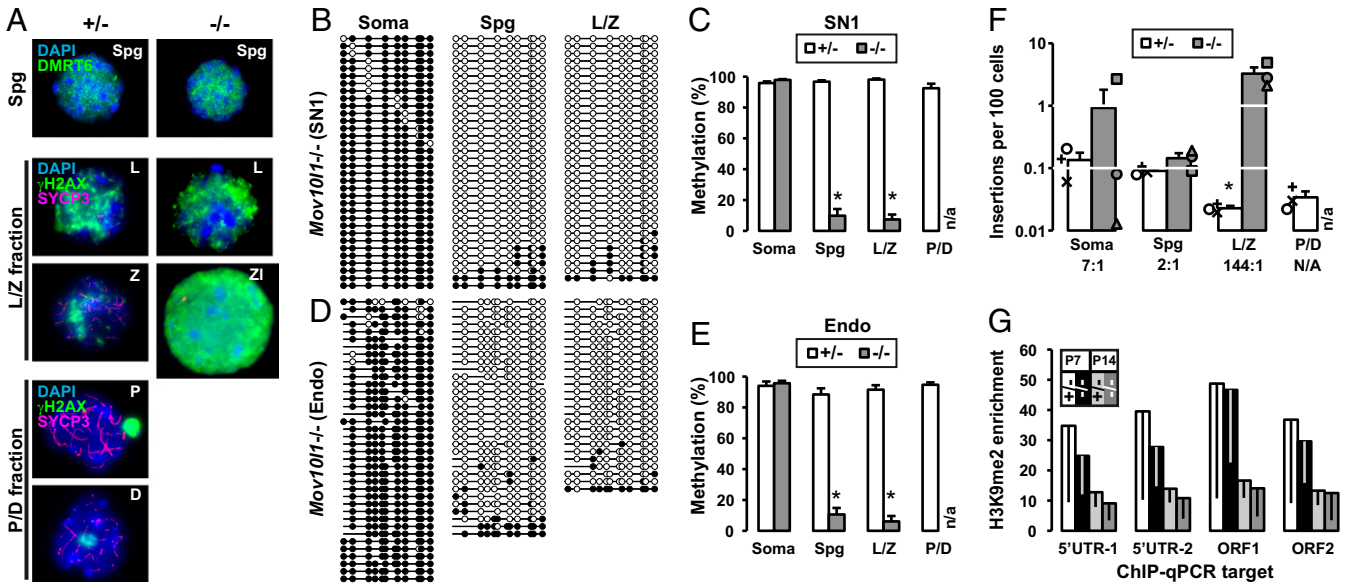

Fig. 4. Characterization of the single-copy 5′UTR-ORFeus transgene in sorted cell fractions from adult testes. (*A*) Immunofluorescence analysis of FACS-enriched cells from *Mov10l1*$^{+/-}$ and *Mov10l1*$^{-/-}$ testes. Nuclear spreads were labeled with either DMRT6 (green) or γH2AX (green)/SYCP3 (magenta) and counterstained with DAPI (blue). Meiotic prophase I staging was determined based on known labeling patterns of these markers. Representative examples are shown for DMRT6^{+} Spg, L/Z fraction, and P/D fraction. Zl, zygotene-like spermatocyte in *Mov10l1*$^{-/-}$ L/Z fraction. All images are at the same scale. (Magnification: 63×.) (*B*) DNA methylation dot plots of transgenic L1 promoter in sorted cell fractions from *Mov10l1*$^{-/-}$ testes. (*C*) Histogram representation of transgenic L1 promoter methylation in both *Mov10l1*$^{+/-}$ and *Mov10l1*$^{-/-}$ testes. (*D*) DNA methylation dot plots of endogenous L1 promoter in sorted cell fractions from *Mov10l1*$^{-/-}$ testes. (*E*) Histogram representation of endogenous L1 promoter methylation in both *Mov10l1*$^{+/-}$ and *Mov10l1*$^{-/-}$ testes. Error bars in *C* and *E* represent SEM between individual sequences. Asterisks indicate statistical difference between two genotypes (Mann–Whitney *U* test, $P < 0.05$). The entire dataset of dot plots corresponding to *C* and *E* are included in Fig. S7. (*F*) Insertion frequency of the transgene in sorted cell fractions from *Mov10l1*$^{+/-}$ and *Mov10l1*$^{-/-}$ testes. The insertion ratio of *Mov10l1*$^{-/-}$ to *Mov10l1*$^{+/-}$ is annotated for each fraction. ddPCR readouts for individual animals are indicated (varied symbols; the same symbol identifies all cell fractions from a specific animal). Error bars represent SEM for biological replicates. Asterisks indicate statistical difference between two genotypes (Student's *t* test, $P < 0.05$). (*G*) H3K9me2 occupancy at endogenous L1 sequences in prepuberal *Mov10l1*$^{+/-}$ and *Mov10l1*$^{-/-}$ testes. Plotted as fold-enrichment over IgG pull-downs for four different regions of the endogenous L1 sequence. Error bars (drawn downward) represent SEM for biological replicates. endo, endogenous; soma, somatic.

sample that had an outlying, relatively higher retrotransposition frequency (2.7 insertions per 100 cells).

The discrepancy between the timing of DNA methylation loss (i.e., in Spg) and the delayed increase in retrotransposition (i.e., in meiotic cells) suggests additional layers of regulation in the spermatogonial population. One candidate is the dimethylation of histone 3 lysine 9 (H3K9me2), which is involved in transcriptional silencing of L1 retrotransposons in Spg (52). This histone modification is developmentally lost as Spg differentiate into meiotic cells in wild-type mice (53). We analyzed the level of H3K9me2 occupancy at endogenous L1 loci as previously reported (53) and observed similar levels of decreases in testicular H3K9me2 abundance from P7 to P14 in both *Mov10l1*$^{+/-}$ and *Mov10l1*$^{-/-}$ genetic backgrounds (Fig. 4*G*). These results suggest that the H3K9me2 pathway remains intact in the Spg of *Mov10l1*$^{-/-}$ mutants.

Inhibition of Retrotransposition Does Not Rescue the Meiotic Phenotype. Thus, far, we have observed a massive increase in retrotransposition frequency by the SN1 transgene in L/Z spermatocytes, a stage immediately preceding the meiotic failure in the *Mov10l1* mutant. The timing of these two events may be a coincidence, but it raises the intriguing possibility that massive retrotransposition precipitates the meiotic arrest. As an attempt to estimate the degree of insertional mutagenesis by endogenous L1s, we extrapolated the frequency of retrotransposition from the reporter transgene to endogenous L1s (Fig. 5*A*). The extrapolation was based on three parameters. The first parameter was the copy number in the genome. The transgene was present at a single copy, whereas there are ∼3,000 copies of potentially active full-length endogenous L1 elements in the mouse genome (54). The second parameter was the ratio of insertion frequencies between the transgene and endogenous L1s. It was set to 200:1 based on retrotransposition assays in cell culture (36). The third parameter was the calculated number of insertions per cell, representing the average mutational burden. The average insertion frequency was 15.1 insertions per 100 cells in P14 testes and 3.3 insertions per 100 cells in L/Z spermatocytes from adults. If we chose the higher frequency from the P14 time point, the transgene would produce 0.15 insertions per cell. If we extrapolated to 3,000 copies of endogenous elements, assuming each is equivalent to the control native element used in the cell-based assay, we would arrive at a frequency of ∼2.3 insertions per cell for endogenous L1s (i.e., $0.15 \times 3{,}000/200 = 2.3$). Considering the random chromosomal distribution of de novo L1 insertions in vivo (25, 27), it is unlikely that insertional mutagenesis is the principle driver of the germ-cell demise. Much higher insertion frequency would be required to imperil all germ cells.

To further test the contribution of increased L1 retrotransposition in the meiotic phenotype, we treated *Mov10l1*$^{-/-}$ animals with a nucleoside reverse-transcriptase inhibitor, dideoxycytidine (ddC), which is highly effective in blocking L1 retrotransposition in cell-based assays (55) (Fig. 5*B*). The control untreated *Mov10l1*$^{-/-}$ animals had an average frequency of 11.7 insertions per 100 cells from the SN1 transgene at P14. Animals treated with a daily dose of 200 mg/kg ddC showed an average of 2.3-fold reduction in retrotransposition. Animals treated with a higher daily dose of 400 mg/kg ddC displayed an average of 4.6-fold reduction (Fig. 5*C*). As expected, *Mov10l1*$^{-/-}$ animals treated with vehicle (PBS) showed no reduction in retrotransposition. Despite apparent inhibition of retrotransposition, histological preparations showed no change in meiotic progression in ddC-treated *Mov10l1*$^{-/-}$ animals (i.e., devoid of pachytene

A

L1 elements	Abundance in the genome (copies)	Insertion frequency per copy	Number of insertions per cell
Transgenic	1	200	0.15
Endogenous	3000	1	2.25

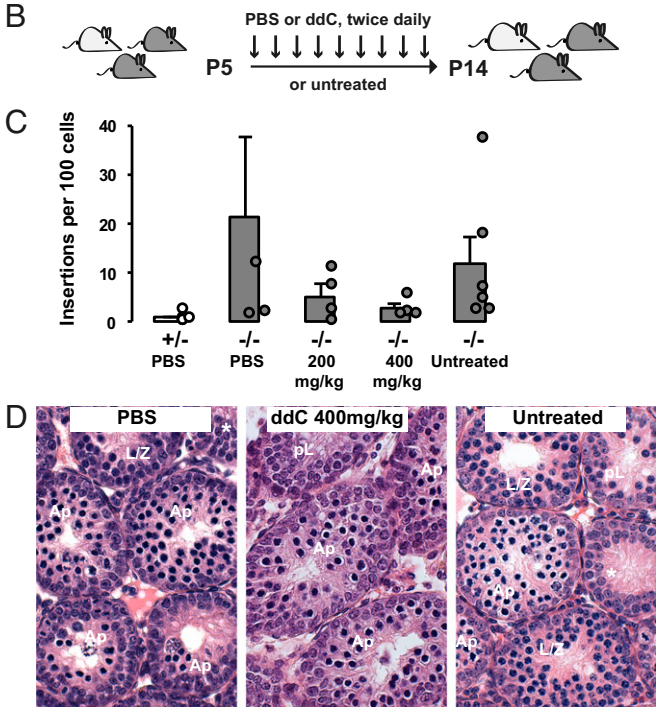

Fig. 5. Pharmacological inhibition of L1 retrotransposition in *Mov10l1*$^{-/-}$ mice. (*A*) Extrapolation of retrotransposition from transgenic to endogenous L1s. See main text for details. (*B*) Treatment scheme. The litter was treated by intraperitoneal injection of the nursing female twice daily from P5 to P14. (*C*) Insertion frequency of the transgene in untreated pups and pups treated with PBS or ddC at two different doses. Except for the first column (light gray), all other columns represent data from *Mov10l1*$^{-/-}$ pups (dark gray). ddPCR readouts for individual animals are indicated (circles) except for one PBS-treated *Mov10l1*$^{-/-}$ mouse, which had 70 insertions per 100 cells. Error bars represent SEM for biological replicates. Note the average insertion frequency trended downward in ddC treated groups but the difference failed to reach statistical significance ($P > 0.05$). (*D*) H&E-stained testicular sections of P14 testes at different treatment conditions. Germ cells of the most advanced stage are labeled for each tubule. Ap, apoptotic spermatocytes; pL, preleptotene. Asterisked tubules lack any discernable spermatocytes. (Magnification: 40×.)

spermatocytes as would be expected for wild-type or *Mov10l1*$^{+/-}$ animals at P14) (Fig. 5*D*).

Discussion

We developed an L1 reporter transgene that is controlled by the endogenous mouse L1 promoter. A hallmark of the mouse model is that the single-copy transgene faithfully recapitulates DNA methylation and RNA expression dynamics of endogenous L1s during male germ-cell development (Fig. 6*A*). First, at the level of DNA methylation, the promoter of the transgene reproduces patterns of endogenous DNA methylation in both the wild-type and a piRNA pathway-deficient background. In the wild-type, the transgenic promoter is demethylated in fetal prospermatogonia and subsequently remethylated in neonatal Spg, as expected for the majority of endogenous mouse L1 promoters (16). In the *Mov10l1*$^{-/-}$ background, the transgenic promoter fails to be remethylated in postnatal germ cells. Our initial analysis in the whole testis indicated that methylation was lost only after P7, but further examination of developmental germ-cell fractions confirmed the lack of remethylation in Spg. These results support a conclusion that, like endogenous L1s reported previously (16), de novo methylation of the single-copy reporter transgene requires the intact piRNA pathway. These data also illustrate the remarkable efficiency of piRNA-directed transcriptional silencing of retrotransposons. In other words, after being introduced into the mouse genome through transgenesis, the piRNA surveillance system was able to identify this single additional copy of the L1 promoter and to target it for de novo DNA methylation.

Second, the transgene reproduces at the RNA level the derepression of endogenous L1s. Previous studies reported a modest ~threefold increase of endogenous L1 transcripts in P10 *Mov10l1*$^{-/-}$ testes (41, 43). Our qRT-PCR data on endogenous L1s are consistent with the published data: no significant increase at P7 but a sixfold increase at P14. Because the qRT-PCR approach cannot discriminate between authentic endogenous L1 transcripts and those cotranscribed within genes (44), we also measured changes at the protein level. In fact, a 10-fold increase in L1 ORF1p is already evident in P7 mutant testes, followed by a 44-fold increase in P14 mutant testes. In this regard, the reporter transgene may offer an advantage because the transgenic RNA can be readily differentiated from the endogenous sequences and

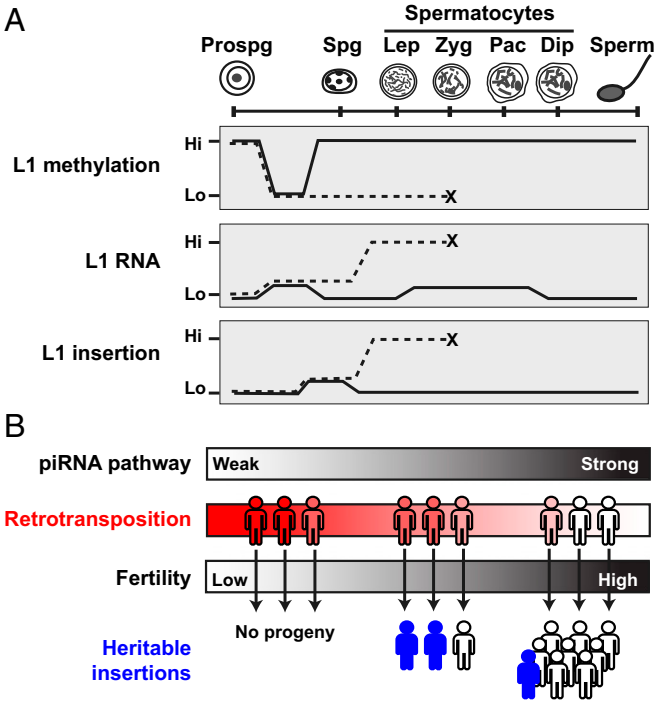

Fig. 6. Model for L1 retrotransposition dynamics and developmental timing. (*A*) Summary of L1 methylation, RNA expression, and retrotransposition during male germ-cell development. Key developmental stages depicted include prospermatogonia (prospg), spermatogonia (spg), L/Z-P/D spermatocytes, and sperm. Solid line represents dynamics observed in *Mov10l1*$^{+/-}$ mice; dashed line represents dynamics in *Mov10l1*$^{-/-}$ mice. For L1 methylation and RNA expression, the depicted dynamics apply to both endogenous L1s and the SN1 transgene. For L1 insertion, the dynamics were observed for the SN1 transgene and are predicted to be applicable to the endogenous L1s. (*B*) Implication of the developmental timing of heritable L1 insertions. The strength of the piRNA pathway is depicted as a quantitative gradient from deficient (weak) to fully functional (strong) because of genetic variations. Accordingly, individuals possess varied retrotransposition potential, ranging from rampant to highly restrained (represented by the filled color gradient). De novo retrotransposition in meiotic germ cells creates unique insertions, which emerge in the next generation as new genetic variants (represented by filled stick figures) if the individual's fertility is not severely compromised.

specifically detected. The overall expression level of the transgene is much lower than that of endogenous L1s (both endogenous and transgene expression levels were normalized to *Gapdh* transcripts and could thus be compared). Similar to endogenous L1s, in the *Mov10l1*$^{-/-}$ background, the transgene displays a stage-specific increase between P7 and P14, albeit at much higher magnitude. In addition, the transgene is already expressed at a 37-fold higher level in *Mov10l1*$^{-/-}$ testes than in *Mov10l1*$^{+/-}$ testes at P7. RNA in situ data provide additional evidence that the increase in RNA expression is primarily in meiotic cells, beginning from leptotene spermatocytes. H3K9me2 cooperates with the piRNA-DNA methylation pathway to transcriptionally silence L1 retrotransposons in Spg (52). We confirmed the enrichment of H3K9me2 in P7 testes compared with P14 under both genetic backgrounds. Thus, the developmentally programmed loss of H3K9me2 in meiotic germ cells accounts for the additional increase in L1 expression in spermatocytes.

Using this model, we were able to quantitatively characterize retrotransposition dynamics and identified a stage-specific increase of retrotransposition in *Mov10l1* mutant meiotic germ cells (Fig. 6*A*). A massive 70-fold increase in retrotransposition was observed at P14, when the majority of the germ cells had entered the first wave of meiosis. Importantly, in adult testes, the increase was only observed in L/Z spermatocytes but not in Spg. Several factors might account for the elevated retrotransposition seen solely in the mutant meiotic germ cells. First, the increase in retrotransposition is in agreement with the magnitude of increase in transgene expression because there is a remarkable accumulation of L1 transgene transcripts at P14 compared with the P7 time point. As stated earlier, an increase in transgene expression is evident at or before P7, although the absolute level of transcripts remains significantly lower than in P14 testes. A similar trend is observed at the L1 protein level (10-fold vs. 44-fold increase of ORF1p in mutant P7 and P14 testes, respectively). These results suggest that L1 expression could be a rate-limiting step and it must exceed a threshold for efficient retrotransposition. Second, spermatocytes may possess some unknown characteristics that render them more susceptible for retrotransposition. As germ cells enter the prophase of meiosis I, they undergo extensive chromatin remodeling (56), which may present a unique chromatin environment that is more conducive to retrotransposition. Indeed, in vitro assays have demonstrated that chromatinization and structural parameters of the DNA target affects the efficiency and specificity of DNA nicking by the human L1 endonuclease (57, 58). In this regard, important insights can be obtained by mapping a large number of insertions in mutant spermatocytes. As each insertion is expected to be unique and only present in a single spermatocyte, extensive optimization of the mapping strategies would be required.

However, despite the massive increase in retrotransposition reported by the transgene, it is unlikely that insertional mutagenesis alone accounts for the *Mov10l1*$^{-/-}$ phenotype. We reasoned that endogenous retrotransposition at the extrapolated frequency of ∼2.3 insertions per cell would not be sufficient to decimate the entire germ-cell population. Note that there are many factors that can affect the accuracy of our extrapolation. For example, we assumed each endogenous copy was equally active. However, retrotransposition competency varied greatly among cloned endogenous L1 loci and only a small subset of endogenous L1 elements had high retrotransposition potential (59). We also did not factor in potential insertional mutagenesis by LTR retrotransposons, such as intracisternal A-type particle (IAP) elements, which are also derepressed in many piRNA-pathway mutants, including *Mov10l1* (12, 13). Moreover, pharmacological inhibition of retrotransposition by ddC failed to rescue the meiotic arrest phenotype. A caveat of the ddC treatment experiment is that the average insertion frequency among treated *Mov10l1*$^{-/-}$ animals remained higher than that in the untreated control *Mov10l1*$^{+/-}$ group. In addition, whether ddC treatment suppresses IAP retrotransposition is unknown. Thus, direct quantification of the degree of endogenous retrotransposition in the mutants is desirable, although the current quantitative approaches are incapable of detecting less than 1% of gain in L1 copies (i.e., ∼30 copies per cell) (22).

It is important to note that our results do not exclude a role of L1 activation in the meiotic phenotype. Instead, it underscores the importance of intermediate processes preceding L1 integration in causing the meiotic defect. L1s may perturb meiotic progression at the level of transcription or translation with respect to the L1 life cycle (13). At the RNA level, aberrant genome-wide transcriptional activation of retrotransposons, as in *Mov10l1*$^{-/-}$ germ cells, may disrupt developmentally programmed cellular processes during meiosis. A recent analysis of the *Dnmt3l* mutant suggests that the loss of DNA methylation at retrotransposon sequences may alter the meiotic chromatin landscape as well as the sites of homologous recombination (22). Unmethylated retrotransposons may also change the expression profile of neighboring genes that are important for meiotic functions, as they can reduce the methylation level at surrounding sites through the formation of sloping shores (45). At the protein level, overexpression of L1 ORF2 protein (ORF2p) is cytotoxic to cultured cells (60–62). In cultured cells, the ORF2p's endonuclease activity generates DNA double-strand breaks (DSBs) (62) but its reverse-transcriptase domain also contributes to cytotoxicity (60, 63). Given the remarkable upregulation of ORF1p in piRNA pathway-deficient spermatocytes, ORF2p overexpression is expected. Indeed, spermatocytes deficient in *Mael* display widespread SPO11-independent DSBs, which are likely mediated by L1 endonuclease activity (64). No SPO11-independent DSBs have been detected in *Dnmt3l*-deficient germ cells (22), suggesting different processes related to L1 activation may be involved for individual mutants. In this regard, pharmacological inhibition of L1 endonuclease is highly desirable but specific inhibitors are not yet available.

The present work highlights the utility of reporter transgenes for studying retrotransposons in vivo. A major advantage is that using reporter transgenes obviates the technical challenge in quantifying copy-number changes from endogenous L1s. We found that the transgene copy number is critical in terms of its regulation by DNA methylation. We previously demonstrated a heterologous promoter for an L1 transgene was hypermethylated when present in the genome as a high-copy tandem array in somatic tissues (47), consistent with a phenomenon known as repeat-induced gene silencing (65). The current work focused on the male germline instead. Interestingly, regardless of the source of the L1 promoter (either human or mouse), tandem-arrayed transgenes resisted DNA methylation erasure during genome-wide embryonic reprogramming. However, the promoters of all transgenes were completely remethylated in postnatal testes, including the human L1 promoter. This observation suggests that the remethylation is the default outcome for transgenic L1 elements in the wild-type background. Because we did not check the methylation status of these tandem-arrayed transgenes in *Mov10l1* mutants, it is unclear whether their remethylation is piRNA-dependent. In contrast, only the single-copy transgene showed a similar level of demethylation in prospermatogonia as endogenous L1s. Thus, for modeling epigenetic regulation in the male germline, it is imperative to use a transgene that is integrated into the mouse genome as a discrete single copy. Additionally, because the SN1 transgene is integrated intronically in *Tnr*, a gene specific to the CNS (37), we do not expect that the transgene expression in germ cells is affected by its genomic location. Thus, the SN1 transgene should be representative of active L1 elements in the mouse genome, allowing simple and sensitive quantification of L1 regulation, expression, and retrotransposition in mouse models.

The stage-specific increase of retrotransposition in *Mov10l1* mutants also provides new insights into the developmental timing of heritable L1 insertions. The relevance of experiments performed in a *Mov10l1*$^{-/-}$ mouse to the native biology of L1s in mammals, including humans, could rightly be questioned. Here we

articulate how in fact this might provide a model for how de novo insertions enter the germline in a population. The frequency of L1 insertion in the human germline has been recently estimated by genomic mapping of dimorphic L1 loci between individuals. De novo insertions appear to be very infrequent (e.g., approximately 1 insertion in every 100–300 live births) (66–68). Accordingly, our limited understanding of the developmental timing of new L1 insertions comes from isolated case reports of pathological insertions in humans (69, 70). The first comprehensive survey was from mouse models using both human and mouse L1-based transgenes, which retrotransposed at relatively low frequencies in somatic tissues (one in 50–500 cells) but even lower in male germ cells (1 in 1,000 cells) (28). In agreement with this pioneer work, we found that testis had the lowest average insertion frequency by the SN1 transgene (0.024 insertions per 100 cells in the wild-type mice) compared with other somatic tissues. Note that the term frequency is defined here as the normalized copy number per cell. It measures cumulative L1 copies in a cell and does not differentiate between de novo insertions in a cell and events occurred in its progenitor. Using the same formula discussed earlier, we estimated the endogenous L1 insertion frequency in the mouse germline to be 1 in 278 cells (e.g., $0.00024 \times 3{,}000/200 = 0.0036$), approximating the calculated low frequency of L1 retrotransposition in humans. Thus, in normal human or mouse individuals, heritable retrotransposition events are incredibly rare.

In contrast, the massive increase of L1 insertions in *Mov10l1* mutants represents the other extreme: much more frequent insertions in germ cells but none can be passed to the next generation because of infertility. A parallel exists in infertile human males with spermatogenic disorders. Such patients are frequently associated with epigenetic inactivation of the piRNA pathway and L1 hypomethylation (71). We propose that the bulk of de novo L1 insertions originate in individuals who possess compromised retrotransposon control but remain fertile or subfertile (Fig. 6*B*). Candidates include those who have a history of cryptorchidism, oligozoospermia, or testicular carcinoma in situ. For example, toddlers afflicted with cryptorchidism often display reduced expression of piRNA-pathway factors and L1 derepression (72). Genetic variants in human PIWI proteins are associated with idiopathic azoospermia or oligozoospermia (73). Both testicular germ-cell tumors and the premalignant testicular tissue adjacent to seminoma show epigenetic inactivation of human PIWI genes and L1 hypomethylation (74). In these individuals, one may expect to see the highest increase in L1 expression in spermatocytes and, consequently, heightened insertion frequency in spermatocytes. Such a scenario has important implications for the mutational potential of new insertions. Because these insertions occur at the final stages of germ-cell development, the selection pressure will act on a limited number of developmental pathways (i.e., postmeiotic development of spermatids into spermatozoa), allowing even deleterious insertions to propagate to the progeny (13). Thus, de novo germline retrotransposition events can be an important source for low frequency, potentially harmful genetic variants that have been identified in the human population by recent large-scale sequencing efforts (75).

Materials and Methods

Detailed materials and methods can be found in *SI Materials and Methods* (76–80). Primer/probes are listed in Dataset S1.

Mice. All SN lines were generated by pronuclear microinjection of linearized pWA125 transgene and maintained by successive backcrossing to B6. The 5′UTR-ORFeus transgene was genotyped with transgene-specific primers following previous PCR conditions (25). SN1 zygosity was determined using a pair of transgenic and locus-specific primers. Animal protocols were approved by Institutional Animal Care and Use Committees at Washington State University and South Dakota State University.

Bisulfite Sequencing. Bisulfite treatment of postnatal or adult DNA was conducted with the EpiTect Plus DNA Bisulfite Kit (Qiagen). Cells collected from embryonic time points were processed by the EpiTect Plus LyseAll Bisulfite Kit (Qiagen). PCR amplification, gel extraction, TA cloning, and sequence analysis were performed as previously described (47).

qRT-PCR. The SN1 transgene expression was quantified using TaqMan Gene Expression Master Mix (Thermo Fisher) and SN1 and *Gapdh* probes in duplex. Endogenous L1 expression was measured using Power SYBR Green PCR Master Mix (Thermo Fisher) and endogenous L1 ORF2 primers (*Gapdh* was measured in separate reactions).

Histology and in Situ RNA Hybridization (RNAscope). For histology, paraffin-embedded sections were stained with H&E at the Sanford Research Molecular Pathology Core. In situ RNA hybridization was performed with an RNAscope 2.0 HD Reagent Red Kit (Advanced Cell Diagnostics) and a custom-made ORFeus ORF1 probe.

Western Blotting. Total protein was extracted from testes, resolved on SDS/PAGE gel, and blotted. For Fig. 3*E*, to control for variability across blots, each membrane was cut into ORF1p and α-tubulin slices. ORF1p slices were probed together with 1:5,000 rabbit anti-ORF1 primary antibody (49, 64). α-Tubulin slices were probed with mouse anti–α-tubulin IgG1 (T5168; Sigma). Signals were quantified by Bio-Rad Image Labs v4.0 with global background subtraction.

ORF1 Immunofluorescence. Testes were fixed in Bouin's fixative, 2 h at room temperature for P0 and P7 and 3 h for P14, and embedded in paraffin. After antigen retrieval, sections were incubated with 1:500 rabbit anti-ORF1 antibody (49, 64) and subsequently with Alexa Fluor 488-conjugated donkey anti-rabbit antibody. Fluorescent images were acquired at identical exposure settings for each channel across samples.

ddPCR. ddPCR reactions contained 40–60 ng of genomic DNA. All reactions were duplexed with EGFP and HPRT TaqMan probes. PCR cycling conditions: 95 °C for 10 min, 40 cycles of 94 °C for 30 s and 60 °C for 1 min, 98 °C for 10 min. Samples were analyzed in Bio-Rad QX200 Droplet Reader using QuantaSoft software v1.3.2.0.

Germ Cell Sorting. For embryonic and neonatal germ cells, mice were crossed with OCT4-EGFP mice (40). Cells were gated according to the GFP fluorescence intensity and cell granularity (see supplemental figure S2 in ref. 45). For isolating germ cells from adult animals, an optimized Hoechst 33342-based flow cytometry protocol (51) was used. Individual mice were used for independent FACS enrichment. Based on immunofluorescence analysis, the purity of FACS-enriched cells was >99% for Soma, 92–95% for Spg, 91–95% for L/Z, and 95–98% for P/D.

ChIP. Immunoprecipitations were performed with mouse anti-H3K9me2 (ab1220; Abcam) and mouse IgG (02–6502; Invitrogen). Quantitative ChIP-PCR was performed with the input DNA as a positive control and IgG precipitated DNA as a negative control. The data were represented as percentage input.

Inhibition of L1 Retrotransposition in Vivo. The dam was treated twice daily via intraperitoneal injection starting from 5 d after the birth of her litter. Dosage was either 200 or 400 mg·kg·d ddC (D5782; Sigma) in 100 μL volume. P14 male pups were killed for analyses.

Data Analysis. Mann–Whitney *U* test was used for DNA methylation and ddPCR data. One-tailed Student's *t* test was used for qRT-PCR and Western blot data. We used an α-level of 0.05 for all statistical tests.

ACKNOWLEDGMENTS. We thank the South Dakota State University Animal Resource Wing for animal care; Jeremy Wang and Phillip Zamore for providing *Mov10l1* mutant mice; and Mary Carlson for editorial assistance. This work was supported by NIH Office of Director Grant R21OD017965 (to W.A.); Eunice Kennedy Shriver National Institute of Child Health and Human Development Grant R21HD080143 (to W.A.); and National Institute of General Medical Sciences (NIGMS) Grant P50GM107632 (to J.D.B. and W.A.). S.J.N. was supported in part by NIGMS Grant T32GM008336. S.L. was supported in part by the State of South Dakota through Biochemical Spatio-Temporal Network Resource (BioSNTR), a South Dakota Research Innovation Center. F.H.G. and M.C.N.M. were supported in part by National Institute of Mental Health Grant R01MH088485. The Sanford Research Molecular Pathology Core was supported by NIGMS Grants P20GM103548 and P20GM103620. W.A. was supported, in part, by the Markl Faculty Scholar Fund. Open Access was funded by BioSNTR.

1. Smit AF (1999) Interspersed repeats and other mementos of transposable elements in mammalian genomes. *Curr Opin Genet Dev* 9:657–663.
2. Waterston RH, et al.; Mouse Genome Sequencing Consortium (2002) Initial sequencing and comparative analysis of the mouse genome. *Nature* 420:520–562.
3. Moran JV, et al. (1996) High frequency retrotransposition in cultured mammalian cells. *Cell* 87:917–927.
4. Dewannieux M, Esnault C, Heidmann T (2003) LINE-mediated retrotransposition of marked Alu sequences. *Nat Genet* 35:41–48.
5. Magiorkinis G, Blanco-Melo D, Belshaw R (2015) The decline of human endogenous retroviruses: Extinction and survival. *Retrovirology* 12:8.
6. Rosser JM, An W (2012) L1 expression and regulation in humans and rodents. *Front Biosci (Elite Ed)* 4:2203–2225.
7. Rodić N, Burns KH (2013) Long interspersed element-1 (LINE-1): Passenger or driver in human neoplasms? *PLoS Genet* 9:e1003402.
8. Miki Y, et al. (1992) Disruption of the APC gene by a retrotransposal insertion of L1 sequence in a colon cancer. *Cancer Res* 52:643–645.
9. Scott EC, et al. (2016) A hot L1 retrotransposon evades somatic repression and initiates human colorectal cancer. *Genome Res* 26:745–755.
10. Kazazian HH, Jr, et al. (1988) Haemophilia A resulting from de novo insertion of L1 sequences represents a novel mechanism for mutation in man. *Nature* 332:164–166.
11. Wimmer K, Callens T, Wernstedt A, Messiaen L (2011) The NF1 gene contains hotspots for L1 endonuclease-dependent de novo insertion. *PLoS Genet* 7:e1002371.
12. Yang F, Wang PJ (2016) Multiple LINEs of retrotransposon silencing mechanisms in the mammalian germline. *Semin Cell Dev Biol* 59:118–125.
13. Newkirk SJ, An W (2017) L1 regulation in mouse and human germ cells. *Human Retrotransposons in Health and Disease*, ed Cristofari G (Springer International, Cham, Switzerland), pp 29–61.
14. Aravin AA, Sachidanandam R, Girard A, Fejes-Toth K, Hannon GJ (2007) Developmentally regulated piRNA clusters implicate MILI in transposon control. *Science* 316:744–747.
15. Kuramochi-Miyagawa S, et al. (2008) DNA methylation of retrotransposon genes is regulated by Piwi family members MILI and MIWI2 in murine fetal testes. *Genes Dev* 22:908–917.
16. Molaro A, et al. (2014) Two waves of de novo methylation during mouse germ cell development. *Genes Dev* 28:1544–1549.
17. Pezic D, Manakov SA, Sachidanandam R, Aravin AA (2014) piRNA pathway targets active LINE1 elements to establish the repressive H3K9me3 mark in germ cells. *Genes Dev* 28:1410–1428.
18. Goh WS, et al. (2015) piRNA-directed cleavage of meiotic transcripts regulates spermatogenesis. *Genes Dev* 29:1032–1044.
19. Watanabe T, Cheng EC, Zhong M, Lin H (2015) Retrotransposons and pseudogenes regulate mRNAs and lncRNAs via the piRNA pathway in the germline. *Genome Res* 25: 368–380.
20. Zhang P, et al. (2015) MIWI and piRNA-mediated cleavage of messenger RNAs in mouse testes. *Cell Res* 25:193–207.
21. Reuter M, et al. (2011) Miwi catalysis is required for piRNA amplification-independent LINE1 transposon silencing. *Nature* 480:264–267.
22. Zamudio N, et al. (2015) DNA methylation restrains transposons from adopting a chromatin signature permissive for meiotic recombination. *Genes Dev* 29:1256–1270.
23. Ostertag EM, et al. (2002) A mouse model of human L1 retrotransposition. *Nat Genet* 32:655–660.
24. An W, et al. (2008) Conditional activation of a single-copy L1 transgene in mice by Cre. *Genesis* 46:373–383.
25. An W, et al. (2006) Active retrotransposition by a synthetic L1 element in mice. *Proc Natl Acad Sci USA* 103:18662–18667.
26. Muotri AR, et al. (2005) Somatic mosaicism in neuronal precursor cells mediated by L1 retrotransposition. *Nature* 435:903–910.
27. Babushok DV, Ostertag EM, Courtney CE, Choi JM, Kazazian HH, Jr (2006) L1 integration in a transgenic mouse model. *Genome Res* 16:240–250.
28. Kano H, et al. (2009) L1 retrotransposition occurs mainly in embryogenesis and creates somatic mosaicism. *Genes Dev* 23:1303–1312.
29. Grandi FC, Rosser JM, An W (2013) LINE-1-derived poly(A) microsatellites undergo rapid shortening and create somatic and germline mosaicism in mice. *Mol Biol Evol* 30:503–512.
30. Aravin AA, et al. (2008) A piRNA pathway primed by individual transposons is linked to de novo DNA methylation in mice. *Mol Cell* 31:785–799.
31. Watanabe T, et al. (2011) Role for piRNAs and noncoding RNA in de novo DNA methylation of the imprinted mouse Rasgrf1 locus. *Science* 332:848–852.
32. Muerdter F, et al. (2012) Production of artificial piRNAs in flies and mice. *RNA* 18:42–52.
33. Yamamoto Y, et al. (2013) Targeted gene silencing in mouse germ cells by insertion of a homologous DNA into a piRNA generating locus. *Genome Res* 23:292–299.
34. Naas TP, et al. (1998) An actively retrotransposing, novel subfamily of mouse L1 elements. *EMBO J* 17:590–597.
35. Han JS, Szak ST, Boeke JD (2004) Transcriptional disruption by the L1 retrotransposon and implications for mammalian transcriptomes. *Nature* 429:268–274.
36. Han JS, Boeke JD (2004) A highly active synthetic mammalian retrotransposon. *Nature* 429:314–318.
37. Weber P, et al. (1999) Mice deficient for tenascin-R display alterations of the extracellular matrix and decreased axonal conduction velocities in the CNS. *J Neurosci* 19: 4245–4262.
38. Hajkova P, et al. (2002) Epigenetic reprogramming in mouse primordial germ cells. *Mech Dev* 117:15–23.
39. Lees-Murdock DJ, De Felici M, Walsh CP (2003) Methylation dynamics of repetitive DNA elements in the mouse germ cell lineage. *Genomics* 82:230–237.
40. Szabó PE, Hübner K, Schöler H, Mann JR (2002) Allele-specific expression of imprinted genes in mouse migratory primordial germ cells. *Mech Dev* 115:157–160.
41. Zheng K, et al. (2010) Mouse MOV10L1 associates with Piwi proteins and is an essential component of the Piwi-interacting RNA (piRNA) pathway. *Proc Natl Acad Sci USA* 107:11841–11846.
42. Vourekas A, et al. (2015) The RNA helicase MOV10L1 binds piRNA precursors to initiate piRNA processing. *Genes Dev* 29:617–629.
43. Frost RJ, et al. (2010) MOV10L1 is necessary for protection of spermatocytes against retrotransposons by Piwi-interacting RNAs. *Proc Natl Acad Sci USA* 107:11847–11852.
44. Deininger P, et al. (2017) A comprehensive approach to expression of L1 loci. *Nucleic Acids Res* 45:e31.
45. Grandi FC, et al. (2015) Retrotransposition creates sloping shores: A graded influence of hypomethylated CpG islands on flanking CpG sites. *Genome Res* 25:1135–1146.
46. Hindson BJ, et al. (2011) High-throughput droplet digital PCR system for absolute quantitation of DNA copy number. *Anal Chem* 83:8604–8610.
47. Rosser JM, An W (2010) Repeat-induced gene silencing of L1 transgenes is correlated with differential promoter methylation. *Gene* 456:15–23.
48. Wang F, et al. (2012) RNAscope: A novel in situ RNA analysis platform for formalin-fixed, paraffin-embedded tissues. *J Mol Diagn* 14:22–29.
49. Branciforte D, Martin SL (1994) Developmental and cell type specificity of LINE-1 expression in mouse testis: Implications for transposition. *Mol Cell Biol* 14:2584–2592.
50. Vergouwen RP, et al. (1993) Postnatal development of testicular cell populations in mice. *J Reprod Fertil* 99:479–485.
51. Gaysinskaya V, Soh IY, van der Heijden GW, Bortvin A (2014) Optimized flow cytometry isolation of murine spermatocytes. *Cytometry A* 85:556–565.
52. Di Giacomo M, Comazzetto S, Sampath SC, Sampath SC, O'Carroll D (2014) G9a co-suppresses LINE1 elements in spermatogonia. *Epigenetics Chromatin* 7:24.
53. Di Giacomo M, et al. (2013) Multiple epigenetic mechanisms and the piRNA pathway enforce LINE1 silencing during adult spermatogenesis. *Mol Cell* 50:601–608.
54. Goodier JL, Ostertag EM, Du K, Kazazian HH, Jr (2001) A novel active L1 retrotransposon subfamily in the mouse. *Genome Res* 11:1677–1685.
55. Dai L, Huang Q, Boeke JD (2011) Effect of reverse transcriptase inhibitors on LINE-1 and Ty1 reverse transcriptase activities and on LINE-1 retrotransposition. *BMC Biochem* 12:18.
56. Crichton JH, Playfoot CJ, Adams IR (2014) The role of chromatin modifications in progression through mouse meiotic prophase. *J Genet Genomics* 41:97–106.
57. Cost GJ, Golding A, Schlissel MS, Boeke JD (2001) Target DNA chromatinization modulates nicking by L1 endonuclease. *Nucleic Acids Res* 29:573–577.
58. Repanas K, et al. (2007) Determinants for DNA target structure selectivity of the human LINE-1 retrotransposon endonuclease. *Nucleic Acids Res* 35:4914–4926.
59. Brouha B, et al. (2003) Hot L1s account for the bulk of retrotransposition in the human population. *Proc Natl Acad Sci USA* 100:5280–5285.
60. Goodier JL, Ostertag EM, Engleka KA, Seleme MC, Kazazian HH, Jr (2004) A potential role for the nucleolus in L1 retrotransposition. *Hum Mol Genet* 13:1041–1048.
61. Belgnaoui SM, Gosden RG, Semmes OJ, Haoudi A (2006) Human LINE-1 retrotransposon induces DNA damage and apoptosis in cancer cells. *Cancer Cell Int* 6:13.
62. Gasior SL, Wakeman TP, Xu B, Deininger PL (2006) The human LINE-1 retrotransposon creates DNA double-strand breaks. *J Mol Biol* 357:1383–1393.
63. Wallace NA, Belancio VP, Deininger PL (2008) L1 mobile element expression causes multiple types of toxicity. *Gene* 419:75–81.
64. Soper SF, et al. (2008) Mouse maelstrom, a component of nuage, is essential for spermatogenesis and transposon repression in meiosis. *Dev Cell* 15:285–297.
65. Garrick D, Fiering S, Martin DI, Whitelaw E (1998) Repeat-induced gene silencing in mammals. *Nat Genet* 18:56–59.
66. Xing J, et al. (2009) Mobile elements create structural variation: Analysis of a complete human genome. *Genome Res* 19:1516–1526.
67. Huang CR, et al. (2010) Mobile interspersed repeats are major structural variants in the human genome. *Cell* 141:1171–1182.
68. Ewing AD, Kazazian HH, Jr (2010) High-throughput sequencing reveals extensive variation in human-specific L1 content in individual human genomes. *Genome Res* 20:1262–1270.
69. Brouha B, et al. (2002) Evidence consistent with human L1 retrotransposition in maternal meiosis I. *Am J Hum Genet* 71:327–336.
70. van den Hurk JA, et al. (2007) L1 retrotransposition can occur early in human embryonic development. *Hum Mol Genet* 16:1587–1592.
71. Heyn H, et al. (2012) Epigenetic disruption of the PIWI pathway in human spermatogenic disorders. *PLoS One* 7:e47892.
72. Hadziselimovic F, Hadziselimovic NO, Demougin P, Krey G, Oakeley E (2015) Piwi-pathway alteration induces LINE-1 transposon derepression and infertility development in cryptorchidism. *Sex Dev* 9:98–104.
73. Gu A, et al. (2010) Genetic variants in Piwi-interacting RNA pathway genes confer susceptibility to spermatogenic failure in a Chinese population. *Hum Reprod* 25:2955–2961.
74. Gainetdinov IV, et al. (2016) Distinguishing epigenetic features of preneoplastic testis tissues adjacent to seminomas and nonseminomas. *Oncotarget* 7:22439–22447.
75. Casals F, Bertranpetit J (2012) Genetics. Human genetic variation, shared and private. *Science* 337:39–40.
76. An W, et al. (2011) Characterization of a synthetic human LINE-1 retrotransposon ORFeus-Hs. *Mob DNA* 2:2.
77. National Research Council (2011) *Guide for the Care and Use of Laboratory Animals* (National Academies Press, Washington, DC), 8th Ed.
78. Tusnády GE, Simon I, Váradi A, Arányi T (2005) BiSearch: Primer-design and search tool for PCR on bisulfite-treated genomes. *Nucleic Acids Res* 33:e9.
79. Zhang T, Murphy MW, Gearhart MD, Bardwell VJ, Zarkower D (2014) The mammalian Doublesex homolog DMRT6 coordinates the transition between mitotic and meiotic developmental programs during spermatogenesis. *Development* 141:3662–3671.
80. Umlauf D, Goto Y, Feil R (2004) Site-specific analysis of histone methylation and acetylation. *Methods Mol Biol* 287:99–120.